

**This is the author version of an article published as:**

**Situ, Rong and Hibiki, Takashi and Sun, Xiaodong and Mi, Ye and Ishii, Mamoru (2004) Axial development of subcooled boiling flow in an internally heated annulus. Experiments in Fluids 37(4):pp. 589-603.**

**Copyright 2004 Springer**

**Accessed from <http://eprints.qut.edu.au>**

## **Axial development of subcooled boiling flow in an internally heated annulus**

**Rong Situ<sup>a</sup>, Takashi Hibiki<sup>a, b, \*</sup>, Xiaodong Sun<sup>a</sup>, Ye Mi<sup>a, 1</sup>, Mamoru Ishii<sup>a</sup>**

<sup>a</sup> *School of Nuclear Engineering, Purdue University, 400 Central Drive, West Lafayette, IN 47907-2017, USA*

<sup>b</sup> *Research Reactor Institute, Kyoto University, Kumatori, Sennan, Osaka 590-0494, Japan*

<sup>1</sup> *Current address: En'Urga Inc., 1291 Cumberland Avenue, West Lafayette, IN 47906, USA*

\* Corresponding author: Tel: +81-724-51-2373, Fax: +81-724-51-2461, Email: hibiki@rri.kyoto-u.ac.jp

**Abstract**-----For the main purpose of the database construction to develop the interfacial area transport equation, axial developments of local void fraction, interfacial area concentration, bubble Sauter mean diameter, interfacial velocity, and bubble number density were measured in boiling water bubbly flows in a vertical-upward internally-heated annulus using a double-sensor conductivity probe. The annulus channel consisted of an inner rod with a diameter of 19.1mm and an outer round tube with an inner diameter of 38.1mm, and the hydraulic equivalent diameter was 19.1 mm. A total of 11 data sets were acquired consisting of four inlet liquid velocities, 0.500, 0.664, 0.987 and 1.22 m/s, two heat fluxes, 100 and 150 kW/m<sup>2</sup>, and two inlet liquid temperatures, 95.0 and 98.0°C. The

axial developments of the flow parameters were discussed based on the measured data in detail. In addition to the database construction, the measured data validated recently proposed constitutive equations for the distribution parameter, drift velocity, and bubble Sauter mean diameter, which will improve the accuracy of the drift-flux model in subcooled bubbly flow.

**Key Words:** Void fraction; Interfacial area concentration; Drift-flux model; subcooled boiling flow; Multiphase flow; Internally heated annulus

## **1. Introduction**

In many energy engineering systems, practical thermal hydraulic phenomena are often dominated by the interfacial transport. Lack of proper mechanistic models for the interfacial structure and interfacial transfer processes leads to inaccurate predictions of these phenomena, and it becomes the major concern in the current two-phase flow modeling practice. Recently, the introduction of the interfacial area transport equation has been recommended to improve the two-fluid model (Kocamustafaogullari and Ishii 1995). It can replace the traditional flow regime maps and regime transition criteria. The changes in the two-phase flow structure are predicted mechanistically by introducing the interfacial area transport equation. Thus, a successful development of the interfacial area transport equation can make a quantum improvement in the two-fluid model formulation.

In the first stage of the development of the interfacial area transport equation,

adiabatic flow was the focus, and the interfacial area transport equation for the adiabatic flow was developed successfully by modeling sink and source terms of the interfacial area concentration due to bubble coalescence and breakup (Wu et al. 1998; Hibiki and Ishii 2000). In the next stage, subcooled boiling flow would be the focus. The extensive literature reviews on subcooled boiling flow research were performed by Rogers and Li (1992), Lee and Bankoff (1998), and Bartel et al. (2001). According to the reviews, many researches have attempted to measure the void fraction in subcooled boiling flows, whereas very few works have been done for the interfacial area concentration measurement. Roy et al. (1994) measured local void fraction, gas velocity and bubble diameter in R-113 boiling flows and Zeitoun et al. (1994) also measured local void fraction, interfacial area concentration and bubble diameter in water boiling flows. In addition to such interfacial area measurements, Lee et al. (2002) recently performed local measurements of the void fraction, gas velocity, and liquid velocity. However, these measurements were conducted at a certain axial location, and thus no data on axial development of local flow parameters, which are very important to evaluate the interfacial area transport equation, have been reported.

From this point of view, the present authors initiated a preliminary local measurement for interfacial area concentration in subcooled boiling water flow in an internally heated annulus (Bartel et al. 2001). In addition to this, some important researches related to the interfacial area transport equation have recently been conducted on (i) separate effect tests using adiabatic air-water flow in an annulus to identify the effect of bubble coalescence and breakup on the interfacial area transport (Hibiki et al. 2003a), (ii)

modeling of bubble-layer thickness to formulate one-dimensional interfacial area transport equation in subcooled boiling flow (Hibiki et al. 2003b), and (iii) modeling of active nucleation site density to identify the boundary condition in subcooled boiling flow (Hibiki and Ishii 2003). In order to develop the reliable interfacial area transport equation, extensive accurate data sets should be collected in various channel geometries, flow regimes, and flow conditions. Nevertheless, no reliable databases have been established to model the interfacial area transport mechanism yet. Thus, this study aims at measuring axial developments of local flow parameters (void fraction, interfacial area concentration, bubble Sauter mean diameter, interfacial velocity and bubble number density) of subcooled boiling bubbly flows in an internally heated annulus. The obtained data are expected to contribute to the database construction of subcooled bubbly flow. In addition to such contribution, the obtained data can also be utilized to evaluate the applicability of the existing distribution parameter, drift velocity, and interfacial area correlations to subcooled bubbly flow. The validated correlations will improve the accuracy of the drift-flux model in subcooled bubbly flow.

## **2. Experimental facility**

The channel geometry and loop design are important if one intends to simulate phenomena in specific industrial equipment. The experimental facility used in the present study was designed to measure the relevant two-phase parameters necessary for developing constitutive models for the two-fluid model in subcooled boiling flow in BWR. It was scaled to a prototypic BWR based on scaling criteria for geometric, hydrodynamic, and

thermal similarities (Bartel et al. 2001). The experimental facility, instrumentation, and data acquisition system are briefly described in this section.

Figure 1 shows the experimental facility layout. The water supply is held in the main tank. The tank is open to the atmosphere through a heat exchanger mounted to the top to prevent explosion or collapse and to degas from the water. There is a cartridge heater inside the tank to heat the water and maintain the inlet water temperature. A cooling line runs inside the tank to provide control of the inlet water temperature and post-experimental cooling of the tank. Water is pumped with a positive displacement, eccentric screw pump, capable of providing a constant head with minimum pressure oscillation. The water, which flows through a magnetic flow meter, is divided into four separate flows and can then be injected into the test section. The test section is an annular geometry that is formed by a clear polycarbonate tube on the outside and a cartridge heater on the inside. The test section is 38.1 mm inner diameter and has a 3.18 mm tube wall thickness, which would ensure the strength of the test tube and the electric resistance to generate specified heat flux. The overall length of the heater is 2670 mm and has a 19.1 mm outer diameter. The heated section of the heater rod is 1730 mm long. The maximum power of the heater is 20 kW, and has a maximum surface heat flux of 0.193 MW/m<sup>2</sup>. The heater rod has one thermocouple that is connected to the process controller to provide feedback control. The heater rod can be traversed vertically to allow many axial locations to be studied with four instrument ports attached to the test section. At each measuring port, there is an electrical double-sensor conductivity probe.

The double-sensor probe methodology was detailed in our previous paper (Hibiki et

al. 2003c). Since the double-sensor probe methodology was developed under the assumption of spherical bubble shape (Wu and Ishii 1999), the double-sensor probe worked very well for relatively small bubbles. However, once cap or slug bubbles are formed, the accuracies of the measurements using a pair of two sensors such as the interfacial area concentration, bubble Sauter mean diameter, and interfacial velocity are generally deteriorated. The criterion of the bubble size is given by the maximum distorted bubble limit,  $D_{d,max}$  (Ishii and Zuber 1979) as

$$D_{d,max} = 4\sqrt{\frac{\sigma}{g\Delta\rho}}, \quad (1)$$

where  $\sigma$ ,  $g$  and  $\Delta\rho$  are the surface tension, the gravitational acceleration, and the density difference between phases, respectively. The maximum distorted bubble limit is estimated to be 10.0 mm at atmospheric pressure (0.101 MPa) and 100 °C. This categorization was approximately made by statistical consideration with the measured bubble chord length. The methodology is detailed in our previous paper (Hibiki et al. 2004). It should be noted here that small number of cap bubbles contained in the flow may not affect the total interfacial area concentration significantly (Hibiki and Ishii 1999). For example, if the ratio of the cap bubble diameter to spherical/distorted bubble diameter is 5 (typical value at bubbly-to-slug flow transition), the contribution of cap bubbles to total interfacial area concentration is less than 2 % for the case that the ratio of cap bubble void fraction to total void fraction is 0.1 (Hibiki and Ishii 1999).

For the bubble diameter smaller than the maximum distorted bubble limit, the measurement accuracies for void fraction, interfacial area concentration, and interfacial

velocity were estimated to be  $\pm 12.8$ ,  $\pm 6.95$ , and  $\pm 12.9$  %, respectively (Hibiki et al. 2003c). Thus, it can be considered that the measurement accuracy of flow parameters would be within  $\pm 15$  % as a conservative estimate. Error bars in figures to be shown later indicate the error band within  $\pm 15$  %.

A pressure tap and thermocouple are placed at the inlet and exit of the test section. A differential pressure cell is connected between the inlet and outlet pressure taps. The two-phase mixture flows out of the test section to a separation tank and the vapor phase is drained away and the water is returned to the holding tank.

The local flow measurements using the double-sensor conductivity probe were performed at four axial locations of  $z_h/D_H=31.3, 52.6, 68.7, \text{ and } 89.4$  as well as 12 radial locations from  $r/(R-R_0)=0.05$  to  $0.95$  under the atmospheric pressure condition. Here,  $z_h$  and  $D_H$  are the axial distance from the start point of heating and the hydraulic equivalent diameter, respectively, and  $r, R,$  and  $R_0$  are the radial location measured from the heater rod surface, the inner radius of the outer tube, and the outer radius of the heater rod, respectively. The flow conditions in this experiment are tabulated in Table 1. In Table 1,  $q, v_{f,in}, T_{in}, \Delta T_{in}, P_{in}$  and  $\Delta P$  are, respectively, the heat flux, the inlet liquid velocity, the inlet liquid temperature, the inlet subcooling, the inlet pressure and the pressure difference between the inlet and the outlet. The measurement accuracies of heat flux, liquid temperature, liquid velocity, pressure, and differential pressure are  $\pm 1\%$ ,  $\pm 0.1^\circ\text{C}$ ,  $\pm 0.1\%$  full-scale reading (1~2 % for present data),  $\pm 1\%$  full-scale reading, and  $\pm 1\%$  full-scale reading, respectively. The pressures at four axial measuring stations are estimated by

considering the gravitational and frictional pressure losses. The gravitational pressure loss can be estimated from the axial one-dimensional void fraction profile obtained by interpolating the void fractions measured at four axial locations. The frictional pressure loss can be estimated by Lockhart-Martinelli's correlation (1949). The prediction accuracy of the outlet pressure is estimated to be within  $\pm 2.88\%$ . Since the axial profiles of the predicted pressures in the present experimental conditions are approximated to be linear, the axial pressures may be estimated by assuming the linear axial pressure profiles with the inlet and outlet pressures. The flow loop and experimental procedure are detailed in our previous report (Ishii et al 2002).

### **3. Results and discussion**

#### **3.1. Void fraction**

Figure 2 shows various profiles of local void fraction,  $\alpha$ , consisting of 12 component figures (3 rows  $\times$  4 columns matrix). In each figure, the void profiles at a fixed axial location are shown as a parameter of heat flux while keeping constant inlet liquid temperature and velocity. Thus, the dependence of the void profile on the heat flux can be seen by comparison between two data sets in each figure. Figures in the first, second and third rows show the void profiles measured at  $z_h/D_H = 31.3, 52.6,$  and  $89.4,$  respectively. The axial development of the void profiles can be seen by comparison among three data sets at the same column. In addition to these, the dependence of the void profiles on the inlet liquid velocity can be seen by comparison between the first, second and third figures from the left at the same row, and the dependence of the void

profiles on the inlet liquid temperature can also be seen by comparison between the second and fourth figures from the left at the same row. In some component figures, some data sets are not shown, which means that no bubble is detected by a double-sensor probe and the flow is still in single liquid phase.

Figure 3 shows axial developments of one-dimensional void fractions,  $\langle \alpha \rangle$  as a function of the thermal equilibrium quality,  $x_{eq}$ , since the thermal equilibrium quality has a clear physical meaning to discuss the thermal effect on the flow parameters. If no heat loss from the test tube and axial heat conduction is assumed,  $x_{eq}$  is estimated by:

$$x_{eq} = \frac{C_{pf} \Delta T_{in}}{h_{fg}} + \frac{q z_h \xi_h}{\rho_f A_c v_{f,in} h_{fg}}, \quad (2)$$

where  $C_{pf}$ ,  $h_{fg}$ ,  $z_h$ ,  $\xi_h$ ,  $\rho_f$ , and  $A_c$  are the liquid specific heat, the latent heat, the heated length, the heated perimeter, the liquid density, and the flow channel cross-section area, respectively. The estimated error of  $x_{eq}$  considering of heat loss is 0.4%. Data at lower qualities correspond to axial locations closer to the channel inlet. The solid and broken lines in Fig.3 indicate the spline interpolations of the one-dimensional void fractions calculated by the following drift-flux model (Hibiki et al. 2003b).

$$\langle \langle v_g \rangle \rangle = \frac{\langle \alpha v_g \rangle}{\langle \alpha \rangle} = \frac{\langle j_g \rangle}{\langle \alpha \rangle} = C_0 \langle j \rangle + V_{gj} = C_0 \left( \frac{G + \Delta \rho \langle j_g \rangle}{\rho_f} \right) + V_{gj}, \quad (3)$$

where  $j_g$ ,  $j$  and  $G$  are the superficial gas velocity, the mixture volumetric flux and the mass flux, respectively. The distribution parameter,  $C_0$ , and the void-fraction-weighted mean drift velocity,  $V_{gj}$ , are given by

$$C_0 = \left(1.2 - 0.2\sqrt{\rho_g/\rho_f}\right) \left[1 - \exp\left(-3.12\langle\alpha\rangle^{0.212}\right)\right], \quad (4)$$

$$V_{gj} = \sqrt{2} \left(\frac{g\sigma\Delta\rho}{\rho_f^2}\right)^{1/4} (1 - \langle\alpha\rangle)^{1.75}, \quad (5)$$

where  $\rho_g$  is the gas density. It should be noted here that Eq.(4) is applicable only to a boiling flow in an internally heated annulus, since the distribution parameter is affected by the channel geometry (Hibiki et al., 2003b). The void fraction can be calculated from Eq.(3) with measured superficial gas velocity and physical properties. The calculation conditions of solid and broken lines in each figure of Fig.3 correspond to experimental conditions of open circle and triangle symbols, respectively. The dotted line in Fig.3 indicates the reference line at  $x_{eq.}=0$ .

The void fraction profiles observed in the present experiments may be characterized as follows.

- (1) A sharp peaking close to the heater surface is observed in each void fraction distribution.
- (2) As will be explained later, the radial location at the maximum void fraction roughly occurs at the distance of the bubble radius from the heater surface.
- (3) As well-known, bubble layer exists in subcooled boiling region. The flow can roughly be characterized as two distinctive flow regions, (i) boiling two-phase (bubble layer) region, and (ii) liquid single-phase region. This indicates that the bubble-layer thickness model can be applicable for formulation of one-dimensional interfacial area transport equation in subcooled boiling two-phase flow (Hibiki et al. 2003b).

- (4) As the bulk subcooling increases along the radial direction, the bubbles collapse and the void fraction drops along the radial direction sharply.
- (5) The void fraction not only increases in value, but also propagates along the radial direction, when (i) the heat flux increases, (ii) the inlet liquid temperature increases, (iii) the inlet liquid velocity decreases, or (iv) the flow develops along the flow direction.

As shown in Fig.3, the one-dimensional void fractions increase along the flow direction mainly due to the phase change, since the maximum pressure difference between  $z_b/D_H=31.3$  and  $89.4$  is less than  $0.01$  MPa. The drift-flux model developed in our previous study (Hibiki et al. 2003b) can reproduce the axial developments of the void fraction very well. The averaged prediction accuracy for all the data listed in Table 1 is estimate to be within  $\pm 6.13$  %. This indicates that the drift-flux model given by Eqs.(3)-(5) can also be applicable to the subcooled boiling flow tested in the present experiment.

The drift-flux model given by Eqs.(3)-(5) is also evaluated by some existing data. Lee et al. (2002) conducted local flow measurements of subcooled water boiling flow in an internally heated annulus. The outer diameter of a heated inner pipe and the inner diameter of an outer pipe were  $19.0$  mm and  $37.5$  mm, respectively. In their experiment, a total of 18 data sets were acquired consisting of the mass flux,  $476$ - $1061$  kg/m<sup>2</sup>s, the heat flux,  $114.8$ - $320.4$  kW/m<sup>2</sup>, and the inlet subcooling,  $11.5$ - $21.3$  °C. The drift-flux model can predict the data within an average relative derivation of  $\pm 4.20$  %. Roy et al. (1994) also performed local flow measurements of subcooled R-113 boiling flow in an internally

heated annulus. The outer diameter of a heated inner pipe and the inner diameter of an outer pipe were 15.9 mm and 38.1 mm, respectively. The experiments were carried out at the mass flux, 579 and 801 kg/m<sup>2</sup>s, the heat flux, 79.4-126.0 kW/m<sup>2</sup>, and the wall temperature 95-102 °C. A total of 7 complete data sets to calculate the distribution parameter are available in the paper. The drift-flux model can predict the data within an average relative derivation of ±10.7 %. Although the available data supports the validity of the drift-flux model given by Eqs.(3)-(5), extensive efforts to take local flow data should be encouraged to evaluate the constitutive equations in a future study.

### **3.2. Interfacial area concentration**

Figure 4 shows various profiles of local interfacial area concentration,  $a_i$ , consisting of 12 component figures (3 rows × 4 columns matrix). The experimental conditions in each figure of Fig.4 are the same as those in the corresponding figure of Fig.2. Since significant cap bubbles are formed in two flow conditions such as  $q=151$  kW/m<sup>2</sup>,  $T_{in}=95$  °C,  $v_{f,in}=0.661$  m/s at  $z_h/D_H=89.4$  and  $q=151$  kW/m<sup>2</sup>,  $T_{in}=98$  °C,  $v_{f,in}=0.992$  m/s at  $z_h/D_H=89.4$ , the corresponding data are not shown in the first and fourth figures from the left at the third row in Fig.4 due to the measurement limitation of the double-sensor probe. Correspondingly, the data of Sauter mean diameter, interfacial velocity, and bubble number density for such conditions will not be shown in the sections of 3.3, 3.4, and 3.5. Figure 5 shows axial developments of one-dimensional interfacial area concentrations,  $\langle a_i \rangle$  as a function of the thermal equilibrium quality,  $x_{eq}$ . The solid and broken lines in Fig.5 indicate the spline interpolations of the one-dimensional interfacial area concentrations

calculated by the semi-theoretical correlation (Hibiki and Ishii 2002).

In the correlation, the flow parameter dependence on the interfacial area concentration was deduced from the interfacial area transport equation considering the hydrodynamic effect on the interfacial area. In the finalization of the bubble Sauter mean diameter correlation, the approximation of  $\langle \alpha \rangle^\Theta \approx \xi \langle \alpha \rangle$  where  $\Theta$  and  $\xi$  are, respectively, the exponent and the coefficient, was made to obtain an advantage such as the direct estimation of the bubble size from easily measurable quantities like superficial fluid velocities. This approximation causes a considerable prediction error of the bubble Sauter mean diameter if we apply the following correlation to  $\langle \alpha \rangle < 0.02$  or  $\langle \alpha \rangle > 0.3$  (Hibiki and Ishii 2002).

$$\langle a_i^* \rangle = 3.02 Lo^{*0.335} \langle \alpha \rangle Re^{*0.239} \quad \text{or} \quad \langle D_{Sm}^* \rangle = 1.99 Lo^{*-0.335} Re^{*-0.239}. \quad (6)$$

where the non-dimensional interfacial area concentration,  $a_i^*$ , Laplace length scale,  $Lo$ , non-dimensional Laplace length scale,  $Lo^*$ , Reynolds number,  $Re^*$ , and the bubble Sauter mean diameter,  $D_{Sm}$ , are defined as follows.

$$a_i^* \equiv a_i Lo, \quad Lo \equiv \sqrt{\frac{\sigma}{g \Delta \rho}}, \quad Lo^* \equiv \frac{Lo}{D_H}, \quad Re^* \equiv \frac{(\varepsilon^{1/3} Lo^{1/3}) Lo}{\nu_f}, \quad \text{and} \quad D_{Sm} \equiv \frac{6\alpha}{a_i}. \quad (7)$$

Here,  $D_H$  and  $\nu_f$  are the hydraulic equivalent diameter and the kinematic viscosity of the liquid phase, respectively. The energy dissipation rate per unit mass,  $\varepsilon$ , may be approximately determined by (Hibiki and Ishii 2002)

$$\varepsilon = g \langle j_g \rangle \exp(-0.0005839 Re_f) + \frac{\langle j \rangle}{\rho_m} \left( -\frac{dP}{dz} \right)_F \left\{ 1 - \exp(-0.0005839 Re_f) \right\}, \quad (8)$$

where  $\rho_m$ ,  $Re_f$  and  $(-dP/dz)_F$  are, respectively, the mixture density defined by  $\rho_g \langle \alpha \rangle + \rho_f (1 - \langle \alpha \rangle)$ , the liquid Reynolds number defined by  $\langle j_l \rangle D_H / \nu_f$ , and the two-phase pressure loss per unit length due to friction which can be estimated by Lockhart-Martinelli's correlation (1949). The correlation of the interfacial area concentration, Eq.(6), can be applicable to extensive loop and flow conditions such as channel geometry (circular or rectangular channel), channel hydraulic equivalent diameter (9.0 mm ~ 5500 mm), flow direction (vertical or horizontal flow), superficial gas velocity (0.000788 m/s ~ 4.87 m/s), and superficial liquid velocity (0.00 m/s ~ 6.55 m/s).

The interfacial area concentration profiles observed in the present experiments may be characterized as follows.

- (1) A sharp peaking close to the heater surface is observed in each interfacial area concentration distribution.
- (2) The radial location at the maximum interfacial area concentration is closer to the heater surface than that at the maximum void fraction. This is attributed to the geometrical relation among the void fraction, interfacial area concentration and bubble Sauter mean diameter, namely,  $a_i = 6\alpha / D_{Sm}$ . As is clear from a simple geometrical consideration of bubbles generated at the heater, the bubble Sauter mean diameter may increase along the radial direction in the vicinity of the heater surface. When the increase rate of the void fraction is smaller than that of the bubble Sauter mean diameter, the peak radial location of the interfacial area concentration appears closer to the heater in comparison with the peak radial location of the void fraction.

- (3) As the bulk subcooling increases along the radial direction, the bubbles collapse and the interfacial area concentration drops along the radial direction sharply.
- (4) The interfacial area concentration not only increases in value, but also propagates along the radial direction, when (i) the heat flux increases, (ii) the inlet liquid temperature increases, (iii) the inlet liquid velocity decreases, or (iv) the flow develops along the flow direction.

As shown in Fig.5, the one-dimensional interfacial area concentrations increase along the flow direction, namely, the thermal equilibrium quality, mainly due to the phase change. The increase rate of the interfacial area concentration in the region of the positive thermal equilibrium quality appears to be lower than that in the region of the negative thermal equilibrium quality due to bubble interaction such as bubble coalescence, which will be discussed in section 3.5. The applicability of the interfacial area correlation given by Eq.(6) to subcooled boiling flows is tested as the first step to develop the interfacial area transport equation, and the correlation works well in the region of the negative thermal equilibrium quality. In the region of the negative thermal equilibrium quality, the phase change due to a strong thermal non-equilibrium is expected, but the phase change may mainly contribute to the bubble volume change, namely the void fraction. In the prediction of the interfacial area concentration, the measured void fractions are used. This may be the reason why the correlation works well even at the thermal non-equilibrium condition. However, since the correlation can not be applicable to cap bubbly and slug flows (Hibiki and Ishii 2002), the correlation tends to overestimate the interfacial area concentration in the region of the positive thermal equilibrium quality due to the formation

of relatively large bubbles. This fact further substantiates the necessity of the interfacial area transport equation to predict such interfacial area transport process accurately. The prediction accuracies of Eq.(6) in the region of the negative thermal equilibrium quality and in the entire tested region listed in Table 1 are estimated to be within  $\pm 22.2\%$  and  $\pm 30.3\%$ , respectively.

### **3.3. Sauter mean diameter**

Figure 6 shows various profiles of local bubble Sauter mean diameter,  $D_{Sm}$ , consisting of 12 component figures (3 rows  $\times$  4 columns matrix). The experimental conditions in each figure of Fig.6 are the same as those in the corresponding figure of Fig.2. Figure 7 shows axial developments of one-dimensional bubble Sauter mean diameter,  $\langle D_{Sm} \rangle$ , as a function of the thermal equilibrium quality,  $x_{eq}$ . The solid and broken lines in Fig.6 indicate the spline interpolations of the one-dimensional bubble Sauter mean diameters calculated by the semi-theoretical correlation, Eq.(6) (Hibiki and Ishii 2002).

The bubble Sauter mean diameter profiles observed in the present experiments may be characterized as follows.

- (1) As bubbles grow near the heater surface, a sharp increase close to the heater surface is observed in the bubble Sauter mean diameter distributions.
- (2) At low void fraction conditions, bubbles collapse in the subcooled bulk region due to high liquid subcooling.
- (3) At higher void fraction condition, such as the condition with  $q=98.1 \text{ kW/m}^2$ ,  $T_{in}=98.0 \text{ }^\circ\text{C}$ , and  $v_{f,in}=0.992 \text{ m/s}$  at  $z_h/D_H=89.4$ , the void fraction keeps dropping along the radial

direction even at the outer half of the channel. However, the bubble diameter is still about 2 mm even in the vicinity of the outer channel wall. This suggests that the bulk temperature is around saturate temperature and thus bubbles would not collapse.

- (4) The bubble Sauter mean diameters increase in value, when (i) the heat flux increases, (ii) the inlet temperature increases, (iii) the inlet liquid velocity decreases, or (iv) the flow develops along the flow direction.

As shown in Fig.7, the one-dimensional bubble Sauter mean diameters increase along the flow direction, namely, the thermal equilibrium quality, mainly due to the phase change and the bubble interaction such as bubble coalescence. The applicability of the bubble Sauter mean diameter correlation given by Eq.(6) to subcooled boiling flows is tested. The correlation appears to give reasonable good predictions of the bubble Sauter mean diameter, but it does not work well at the flow conditions where the one-dimensional void fraction is lower than 0.02 (see Fig.3) and the thermal equilibrium quality is around zero or positive. To discuss the deviations between the correlation and the data, the flow conditions can roughly be classified into three regions, namely (i) the void fraction lower than 0.02 where a strong thermal non-equilibrium is expected, (ii) the void fraction higher than 0.02 and the thermal equilibrium quality lower than zero and (iii) the thermal equilibrium quality equal to or higher than zero. The correlation appears to work well in the region (ii). The reason can be explained as follows:

To develop a general correlation of the bubble diameter, hydrodynamic and thermal effect on the bubble diameter should be taken into account. However, Eq.(6) only took account of the hydrodynamic effect (Hibiki and Ishii 2002). Thus, as the void

fraction decreases to zero, the calculated bubble Sauter mean diameter does not approach zero. This is true for an adiabatic flow, but this may not be the case for a boiling flow. Thus, for a strong thermal non-equilibrium condition (i) where the thermal effect is more pronounced, the correlation may not work well. However, for the condition such that the hydrodynamic effect is dominant, corresponding to the region (ii) in this experiment, the correlation appears to work well. In the region (iii), Eq.(6) tends to underestimate the bubble diameter. This indicates that bubble coalescence much more than the prediction by Eq.(6) may occur. This may be due to more localized bubbles near the heater resulting in the bubble coalescence much enhanced than that for the bubbles distributed uniformly over the flow channel at the same one-dimensional void fraction. The prediction accuracies of Eq.(6) in the region (i) and in the entire region tested in Table 1 are estimated to be within  $\pm 13.7\%$  and  $\pm 31.7\%$ , respectively.

The constitutive equation of the bubble Sauter mean diameter, Eq.(6) is also evaluated by the R-113 data taken by Roy et al. (1994). Only one complete datum to calculate the bubble Sauter mean diameter and the other flow parameters is available at the mass velocity of  $801 \text{ kg/m}^2\text{s}$ , the heat flux of  $115.8 \text{ kW/m}^2$ , and the inlet R-113 temperature of  $43.0 \text{ }^\circ\text{C}$ . Equation (6) can predict the bubble Sauter mean diameter with a relative derivation of  $\pm 25.0\%$ . Although the available datum supports the validity of Eq.(6), extensive efforts to take local flow data should be encouraged to improve the constitutive equation in a future study.

### **3.4. Interfacial velocity**

Figure 8 shows various profiles of local interfacial velocity,  $v_i$ , consisting of 12 component figures (3 rows  $\times$  4 columns matrix). The experimental conditions in each figure of Fig.8 are the same as those in the corresponding figure of Fig.2. Figure 9 shows axial developments of the one-dimensional interfacial velocity,  $\langle\langle v_i \rangle\rangle_a$ , as a function of the thermal equilibrium quality,  $x_{eq}$ . The solid and broken lines in Fig.8 indicate the spline interpolations of one-dimensional interfacial velocity calculated by the drift-flux model, Eq.(3) (Hibiki et al. 2003b).

The interfacial velocity profiles observed in the present experiments may be characterized as follows.

- (1) The local interfacial velocity profiles are found to be almost flat in the region where the radial location is roughly smaller than the maximum bubble Sauter mean diameter, namely,  $r \leq D_{Sm,max}$ . Since the bubbles in the region are expected to slide on the heater surface, the flat interfacial velocity in the bubble-layer region may mainly be due to the sliding bubbles on the heater surface.
- (2) For  $r \geq D_{Sm,max}$ , the interfacial velocity gradually increases along the radial direction, and may reach its maximum value around the channel center. The inlet liquid Reynolds number,  $Re_f$ , varies in the experiments from 28,870 to 70,260, which means that the flows are essentially turbulent flow. Thus, the liquid velocity profile is expected to be quite flat around the channel center. Therefore, the increase in the interfacial velocity along the radial direction around the channel center may not be so significant.

As shown in Fig.8, the one-dimensional interfacial velocities increase along the flow direction, namely, the thermal equilibrium quality, mainly due to the propagation of

the bubble layer region towards the wall of the outer tube. The bubbles in the channel core region can rise faster than those in the channel wall region, resulting in the increased interfacial velocity by increasing the thermal equilibrium quality. After the bubble layer region reach the wall of the outer tube, the axial change of the interfacial velocity appears to be insignificant.

The interfacial velocity,  $\langle\langle v_i \rangle\rangle_a (\equiv \langle v_i a_i \rangle / \langle a_i \rangle)$ , can be approximated by  $\langle\langle v_g \rangle\rangle (\equiv \langle v_g \alpha \rangle / \langle \alpha \rangle)$  in the bubbly flow regime (Wu et al. 1998; Hibiki and Ishii 2000). The drift-flux model developed in our previous study (Hibiki et al. 2003b) can reproduce the axial developments of the interfacial velocity very well. The averaged prediction accuracy for all the data listed in Table 1 is estimated to be within  $\pm 5.92\%$ . This indicates the drift-flux model given by Eqs.(3)-(5) can also be applicable to the subcooled boiling flow tested in the present experiment.

As explained above, axial developments of local void fraction, interfacial area concentration, bubble Sauter mean diameter, and interfacial velocity have been measured in boiling water bubbly flows in a vertical-upward internally-heated annulus using the double-sensor conductivity probe. The clear understanding has been obtained for the mechanisms of the profiles of local flow parameters and the axial developments. All of the data sets are also shown in our previous report (Ishii 2002). The data from the double-sensor probe give near complete information on the time-averaged local hydrodynamic parameters of bubbly two-phase flow. These data will eventually be used for the development of reliable constitutive relations which reflect the true transfer mechanisms in subcooled bubbly flow.

### **3.5. Bubble number density**

Figure 10 shows various profiles of local bubble number density,  $N_b$ , consisting of 12 component figures (3 rows  $\times$  4 columns matrix). The experimental conditions in each figure of Fig.10 are the same as those in the corresponding figure of Fig.2.

The bubble number density profiles observed in the present experiments may be characterized as follows.

- (1) A sharp peaking close to the heater surface is observed in each bubble number density distribution.
- (2) The bubble number density not only increases in value, but also propagates along the radial direction, when (i) the heat flux increases, (ii) the inlet liquid temperature increases, (iii) the inlet liquid velocity decreases, or (iv) the flow develops along the flow direction.

In some conditions, bubble coalescence, which reduces the bubble number density and interfacial area concentration, appears to occur, which reduce the bubble number density and interfacial area concentration. To discuss the bubble coalescence phenomena, Fig.11 compares radial profiles of void fraction, interfacial area concentration and bubble number density at  $z_h/D_H = 52.6$  and  $68.7$ . As an example, the radial profiles measured at  $q = 99.2 \text{ kW/m}^2$ ,  $T_{in} = 98.0^\circ\text{C}$ , and  $v_{fi} = 0.502 \text{ m/s}$  are shown in Fig.11. Figure 11 clearly shows that the void fraction increases along the flow direction, while the interfacial area concentration and the bubble number density decrease along the flow direction. This may exemplify the occurrence of the bubble coalescence, which certainly decreases the

interfacial area concentration and the bubble number density.

#### **4. Conclusions**

Accurate prediction of the interfacial area concentration is essential to successful development of the interfacial transfer terms in the two-fluid model. Mechanistic modeling of the interfacial area concentration entirely relies on accurate local flow measurements over extensive flow and thermal conditions. From this point of view, accurate measurement of flow parameters such as void fraction, interfacial area concentration, bubble Sauter mean diameter, interfacial velocity, and bubble number density were performed by a double-sensor probe in vertical upward subcooled boiling bubbly flows using an internally heated annulus. The obtained results are summarized as follows:

- (1) The local measurements were performed at four axial locations of  $z_h/D_H=31.3, 52.6, 68.7, \text{ and } 89.4$  as well as 12 radial locations from  $r/(R-R_0)=0.05$  to 0.95 using a double sensor probe. A total of 11 data sets were acquired consisting of four inlet liquid velocities, 0.500, 0.664, 0.987, and 1.22 m/s, two heat fluxes, 100 and 150 kW/m<sup>2</sup>, and two inlet liquid temperatures, 95.0 and 98.0°C.
- (2) The phenomena characterizing the subcooled boiling bubbly flows were discussed in detail.
- (3) The mechanisms of the radial profiles of local flow parameters and their axial developments were briefly discussed.

- (4) The existing drift-flux model was compared with the measured one-dimensional data. It reproduced the axial developments of the void fraction and interfacial velocity very well. The averaged prediction accuracies of one-dimensional void fraction and interfacial velocity were estimated to be within  $\pm 6.13\%$  and  $\pm 5.92\%$ , respectively.
- (5) The existing interfacial area correlation was compared with the measured one-dimensional data. It reproduced the axial developments of the interfacial area concentration very well in the region of the negative thermal equilibrium quality. The prediction accuracies of the correlation in the region of the negative thermal equilibrium quality and in the entire tested region were estimated to be within  $\pm 22.2\%$  and  $\pm 30.3\%$ , respectively.
- (6) The existing bubble Sauter mean diameter correlation was compared with one-dimensional data. The prediction accuracies of the correlation in the region of the negative thermal equilibrium quality and  $\langle \alpha \rangle > 0.02$  and in the entire tested region were estimated to be within  $\pm 13.7\%$  and  $\pm 31.7\%$ , respectively.

The data from the double-sensor probe give near complete information on the time-averaged local hydrodynamic parameters of bubbly two-phase flow. These data will eventually be used for the development of reliable constitutive relations which reflect the true transfer mechanisms in subcooled bubbly flow.

## **Acknowledgments**

The research project was supported by the Tokyo Electric Power Company

(TEPCO). The authors would like to express their sincere appreciation for the support and guidance from Dr. Mori of the TEPCO.

## **References**

- Bartel MD, Ishii M, Masukawa T, Mi Y, Situ R (2001) Interfacial area measurements in subcooled flow boiling. *Nucl. Eng. Des.* 210: 135-155
- Hibiki T, Ishii M (1999) Experimental study on interfacial area transport in bubbly two-phase flows. *Int. J. Heat Mass Transfer* 42: 3019-3035
- Hibiki T, Ishii M (2000) One-group interfacial area transport of bubbly flows in vertical round tubes. *Int. J. Heat Mass Transfer* 43: 2711-2726
- Hibiki T, Ishii M (2002) Interfacial area concentration of bubbly flow systems, *Chem. Eng. Sci.* 45: 707-721
- Hibiki T, Ishii M (2003) Active nucleation site density in boiling systems, *Int. J. Heat Mass Transfer* 46: 2587-2601
- Hibiki T, Goda H, Kim S, Ishii M, Uhle J (2004) Structure of vertical downward bubbly flow, *Int. J. Heat Mass Transfer* 47: 1847-1862
- Hibiki T, Situ R, Mi Y, Ishii M (2003a) Experimental study on interfacial area transport in vertical upward bubbly two-phase flow in an annulus. *Int. J. Heat Mass Transfer* 46: 427-441
- Hibiki T, Situ R, Mi Y, Ishii M (2003b) Modeling of bubble-layer thickness for formulation of one-dimensional interfacial area transport equation in subcooled boiling two-phase flow. *Int. J. Heat Mass Transfer* 46: 1409-1423

- Hibiki T, Situ R, Mi Y, Ishii M (2003c) Local flow measurements of vertical upward bubbly flow in an annulus. *Int. J. Heat Mass Transfer* 46: 1479-1496
- Ishii M, Situ R, Hibiki T, Mi Y, Sun X (2002) Experimental and theoretical investigation of subcooled boiling for numerical simulation Progress report 6 (Final report). Purdue University Nuclear Engineering Technical Report, PU/NE-02-11
- Ishii M, Zuber N (1979) Drag coefficient and relative velocity in bubbly, droplet or particulate flows, *AIChE J.* 25: 843-855
- Kocamustafaogullari G, Ishii M (1995) Foundation of the interfacial area transport equation and its closure relations. *Int. J. Heat Mass Transfer* 38: 481-493
- Lee SC, Bankoff SG (1998) A comparison of predictive models for the onset of significant void at low pressures in forced-convection subcooled boiling. *KSME Int. J.* 12: 504-513
- Lee TH, Park GC, Lee DJ (2002) Local flow characteristics of subcooled boiling flow of water in a vertical concentric annulus. *Int. J. Multiphase Flow* 28: 1351-1368
- Lockhart RW, Martinelli RC (1949) Proposed correlation of data for isothermal two-phase, two-component flow in pipes. *Chem. Eng. Prog.* 5: 39-48
- Rogers JT, Li J (1992) Prediction of the onset of significant void in flow boiling of water. ASME Paper HTD-217, *Fundamentals of Subcooled Flow Boiling*: 41-52
- Roy RP, Velidandla V., Kalra SP, Peturaud P (1994) Local measurement in the two-phase region of turbulent subcooled boiling flow. *J. Heat Transfer* 116: 660-669
- Wu Q, Ishii M (1999) Sensitivity study on double-sensor conductivity probe the measurement of interfacial area concentration in bubbly flow. *Int. J. Multiphase Flow* 25: 155-173

Wu Q, Kim S, Ishii M, Beus SG (1998) One-group interfacial area transport in vertical bubbly flow. *Int. J. Heat Mass Transfer* 41: 1103-1112

Zeitoun O, Shoukri, M, Chatoorgoon V. (1994) Measurement of interfacial area concentration in subcooled liquid-vapour flow. *Nucl. Eng. Design* 152: 243-255

**Table 1**

**Flow conditions in this experiment.**

$q$ [kW/m <sup>2</sup> ]	$v_{fi}$ [m/s]	$T_{in}$ [°C]	$\Delta T_{in}$ [°C]	$P_{in}$ [kPa]	$\Delta P$ [kPa]
99.6	0.498	95.0	11.7	32.8	19.1
99.2	0.502	98.0	8.3	30.8	16.5
98.7	0.665	95.0	11.9	33.7	22.1
151	0.662	95.0	11.9	33.7	29.9
99.6	0.970	95.0	12.6	36.8	16.8
149	0.994	95.0	12.6	36.7	20.1
98.1	0.997	98.0	9.8	37.8	20.2
151	0.987	98.0	9.9	38.3	19.9
101	1.190	95.0	13.1	39.0	12.7
150	1.240	95.0	12.8	37.5	21.0
150	1.230	98.0	10.4	40.4	20.6

### **Captions of Figures**

**Fig.1.** Schematic diagram of experimental loop

**Fig.2.** Local void fraction profiles

**Fig.3.** Axial developments of one-dimensional void fraction

**Fig.4.** Local interfacial area concentration profiles

**Fig.5.** Axial developments of one-dimensional interfacial area concentration

**Fig.6.** Local bubble Sauter mean diameter profiles

**Fig.7.** Axial developments of one-dimensional bubble Sauter mean diameter

**Fig.8.** Local interfacial velocity profiles

**Fig.9.** Axial developments of one-dimensional interfacial velocity

**Fig.10.** Local bubble number density profiles

**Fig.11.** Axial developments of local void fraction, interfacial concentration and bubble number density.

Fig. 1

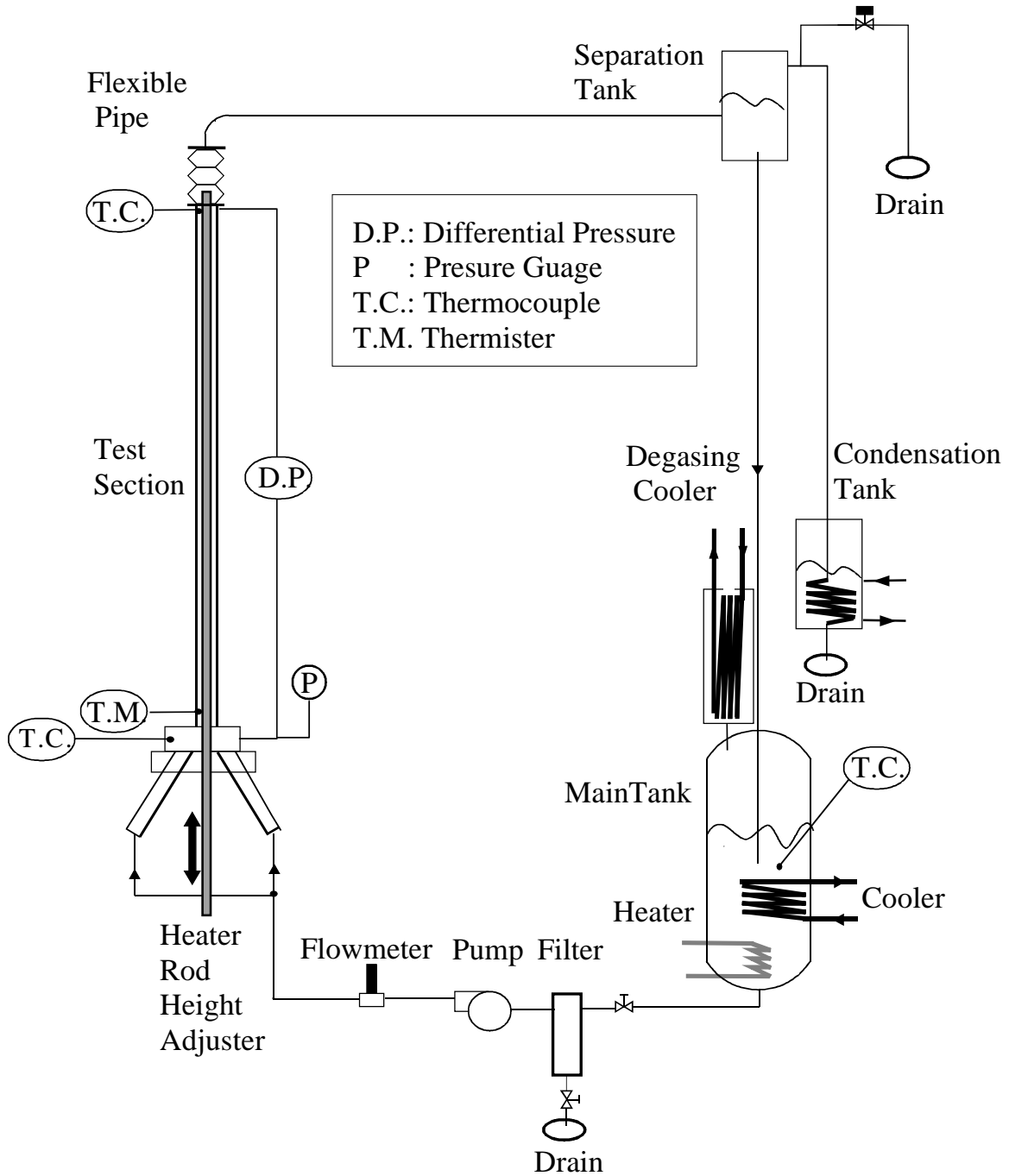


Fig. 2

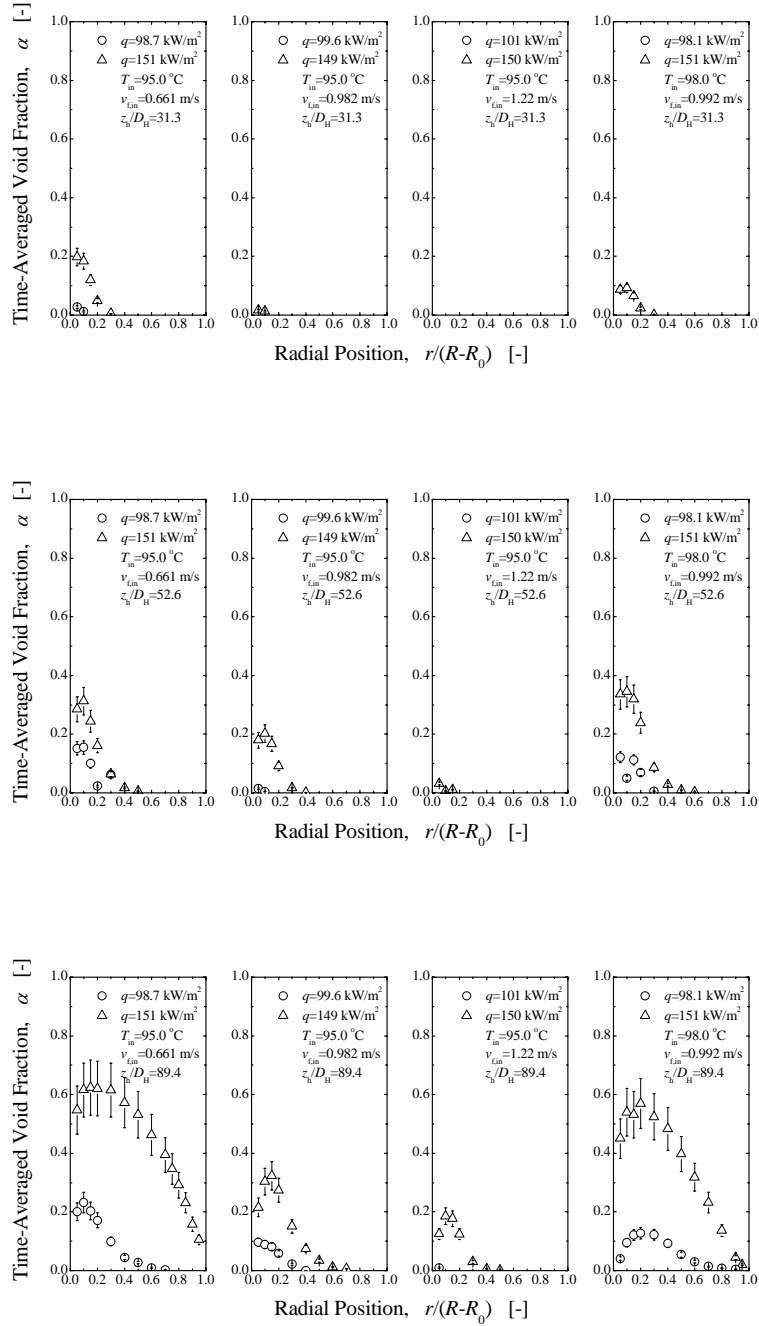


Fig.3

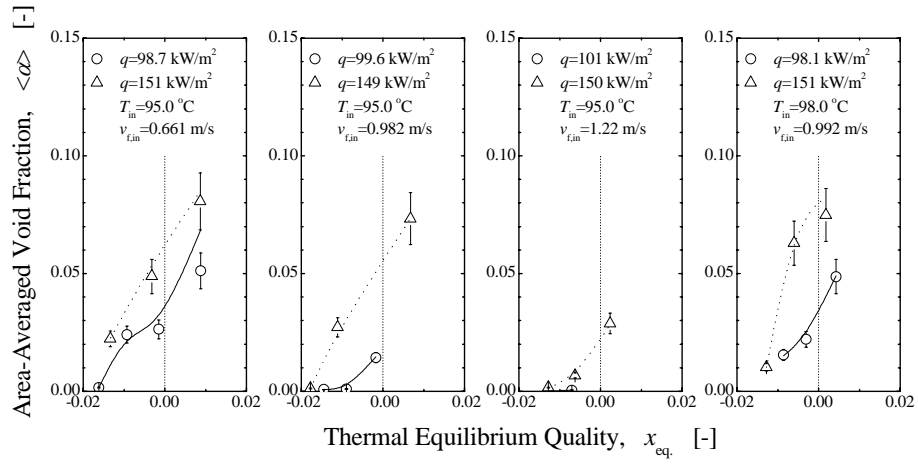


Fig.4

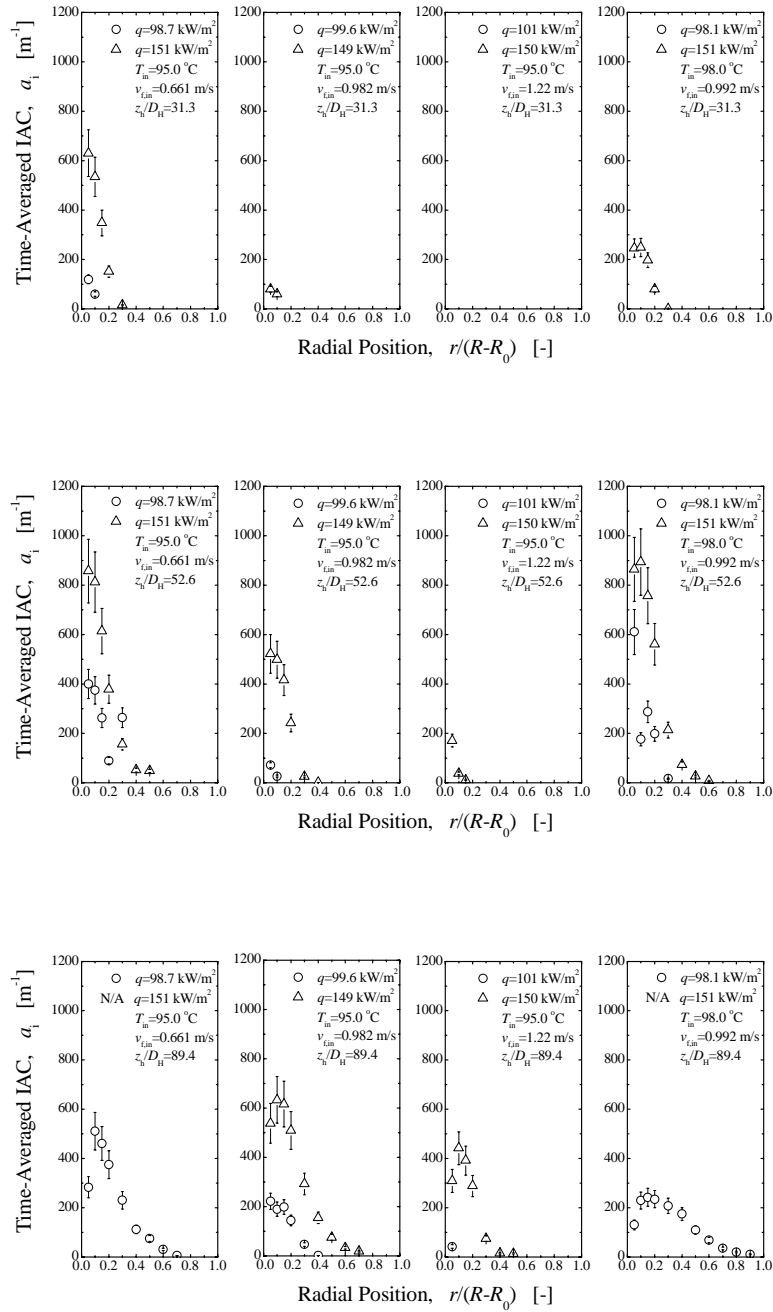


Fig.5

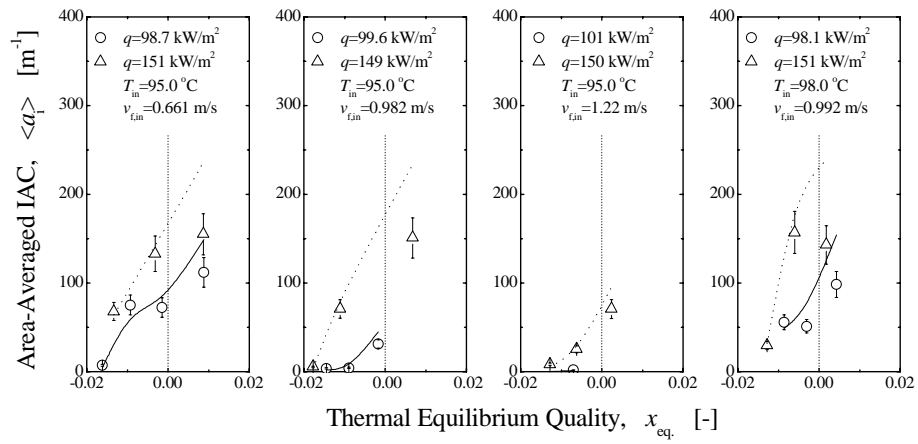


Fig.6

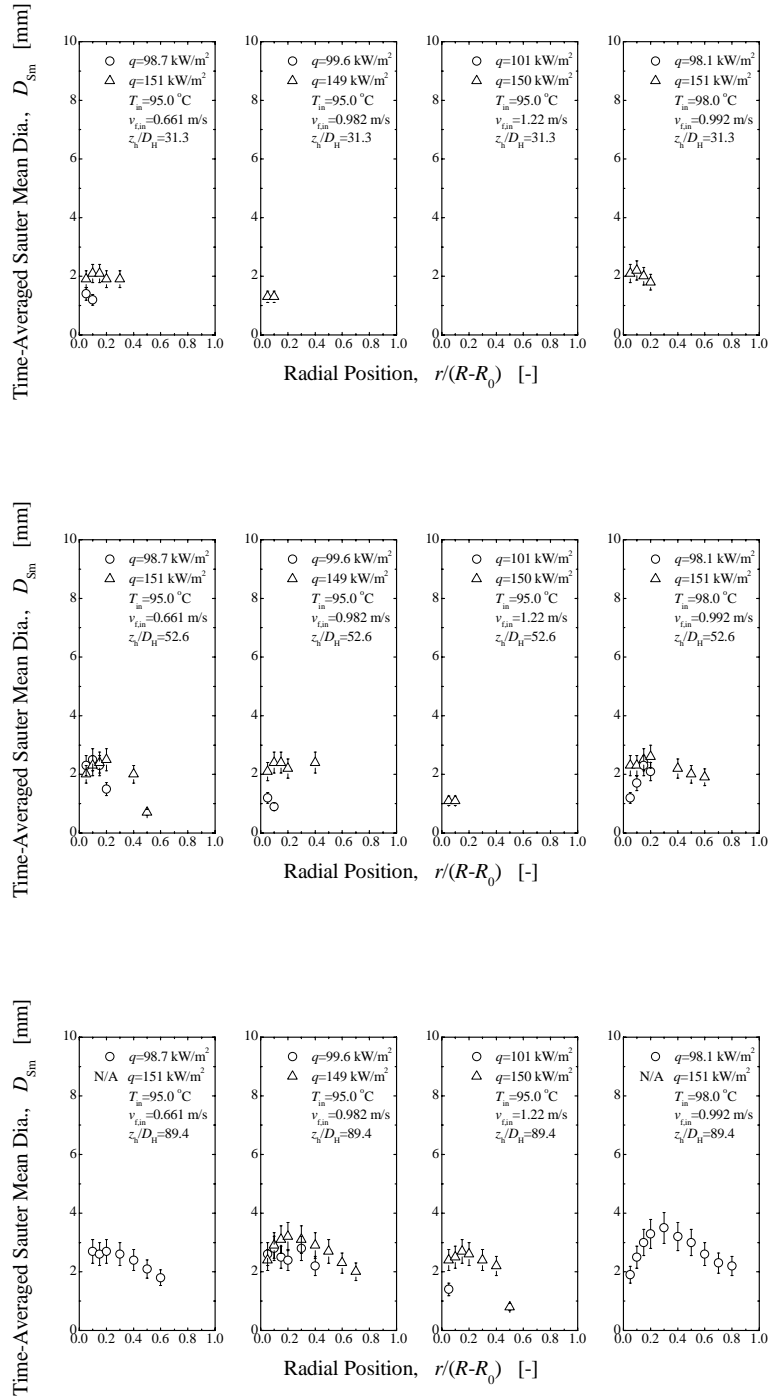


Fig.7

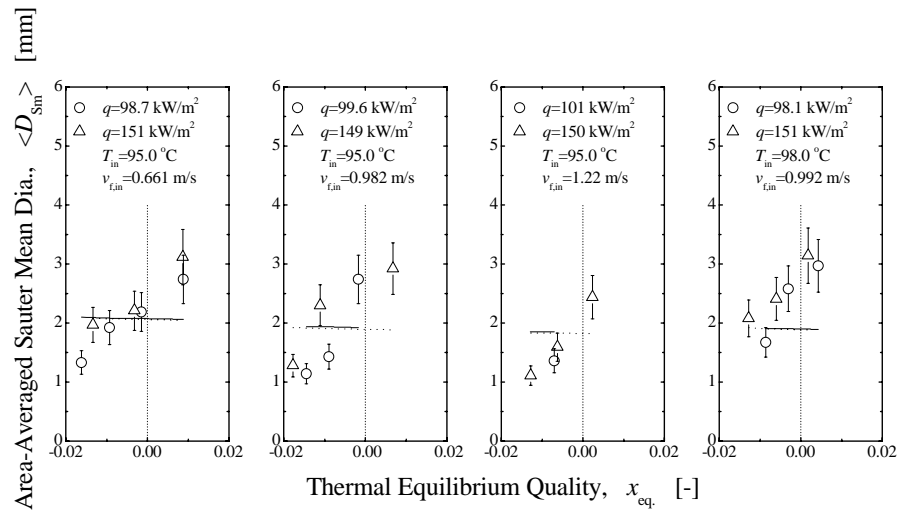
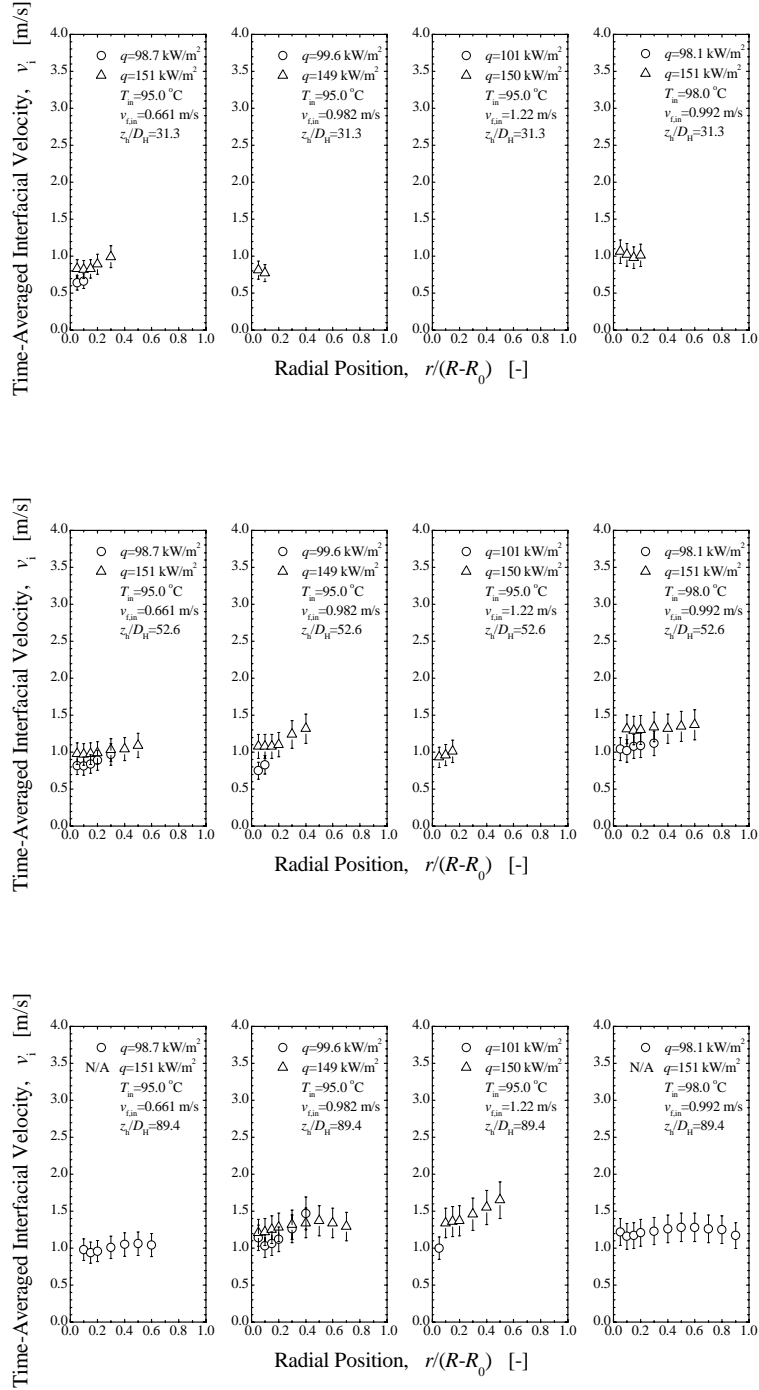


Fig.8



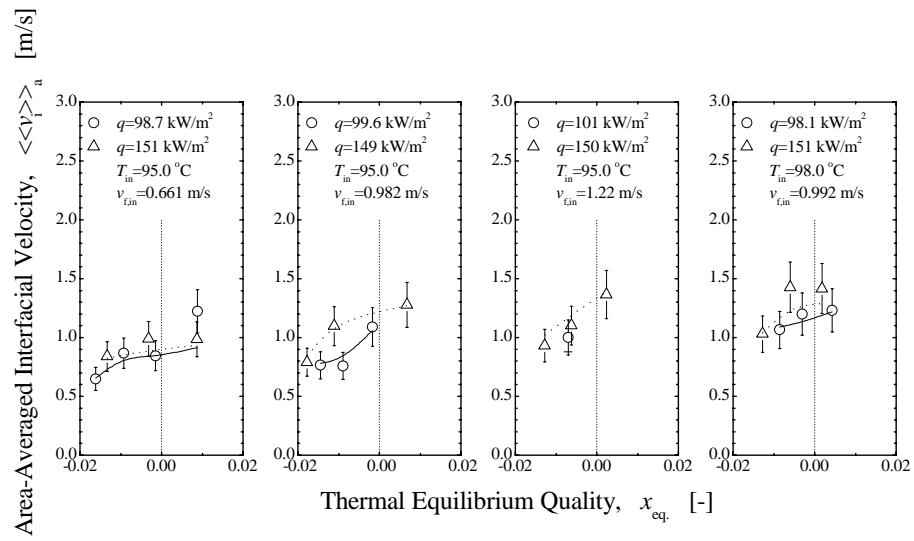


Fig.9

Fig.10

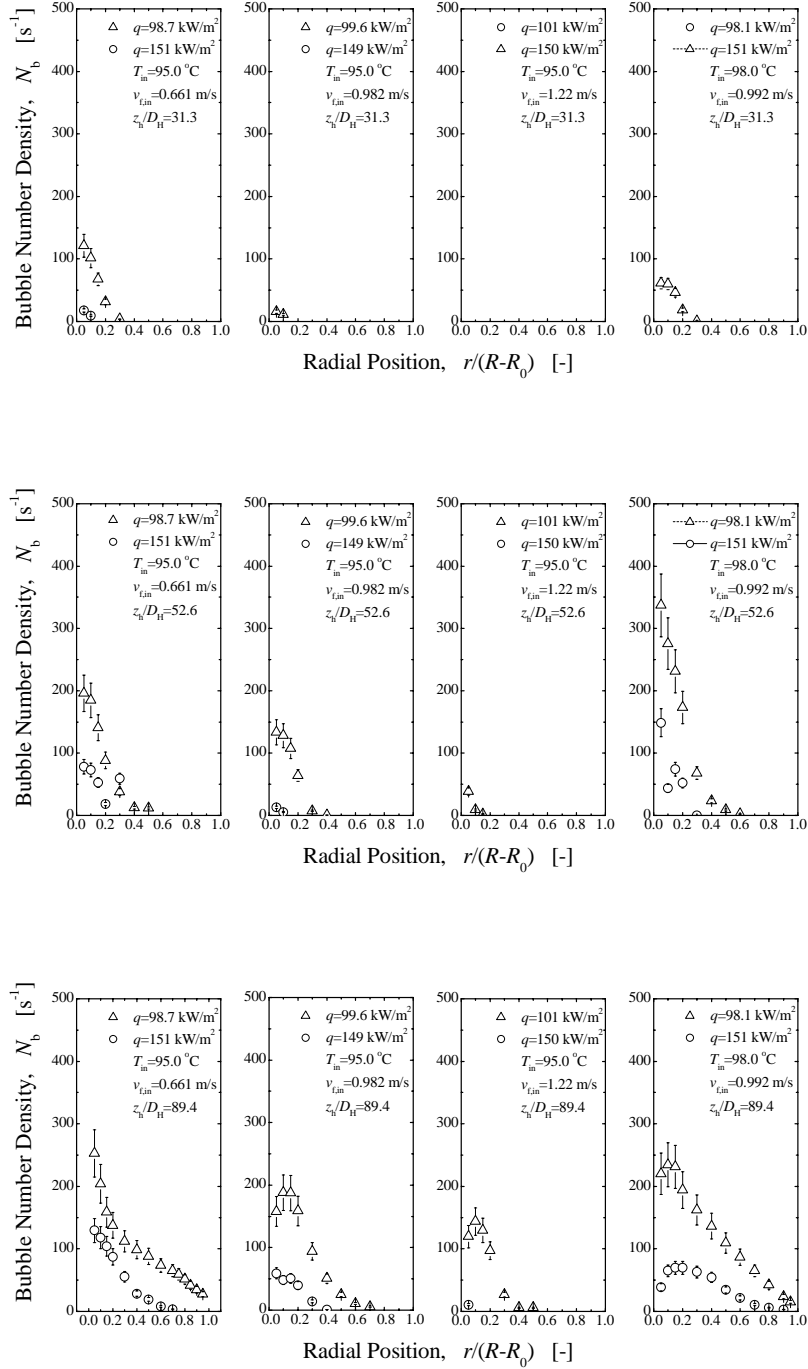


Fig.11

